Distribution Power Loss Mitigation of Parallel-Connected Distributed Energy Resources in Low-Voltage DC Microgrids Using a Lagrange Multiplier-Based Adaptive Droop Control

Yajie Jiang, Yun Yang, *Member, IEEE*, Siew-Chong Tan, *Senior Member, IEEE*, and Shu-Yuen Ron Hui, *Fellow, IEEE*

***Abstract*—This article presents a Lagrange multiplier-based adaptive droop control to mitigate distribution power loss of parallel-connected distributed energy resource (DER) systems in dc microgrids. The distribution power loss comprising line loss and converter loss can be modeled as a quadratic function of the output currents of the DER systems, which can be optimized by the tertiary-layer Lagrange multiplier method to obtain the optimal output current references for the secondary-layer adaptive droop control. The output currents are compensated by the adaptive droop control to provide output voltage references for the primary-layer local dual-loop control, which is a conventional local control scheme for the regulations of grid-connected dc–dc converters. Both simulation and experimental results validate that the proposed control strategy can reduce the distribution power loss of parallel-connected DER systems in 48 V dc microgrids as compared to the conventional control strategy by only optimizing the line loss in different cases.**

***Index Terms*—Adaptive droop control, distribution power loss, distributed energy resource (DER), dc microgrid, Lagrange multiplier method.**

I. Introduction

IN LOW-VOLTAGE dc microgrids, high distribution power loss of distributed energy resources (DER) is a prominent issue that can deteriorate efficient operations of microgrid systems [1]–[6]. The distribution power loss may not only degrade power transfer efficiency of DER systems but also increase the cooling system costs [7]. To this end, pioneering researchers have investigated numerous control strategies to mitigate distribution power loss of DER systems [8]–[23].

Optimal dispatches of DER systems based on the power flow model is a widely adopted strategy to reduce the distribution power loss [8]–[11]. However, most of the dispatches are conducted offline. Alternatively, model-based optimization strategies are conducted online [12]–[23]. The distribution power loss of the model-based optimization strategies is established based on the output voltages of DER systems and the line resistances between the DER systems and dc buses. The output voltages and power of DER systems are controlled to reduce the line loss by considering power generation limits, power flow constraints, state-of-charge of batteries, etc. [12]–[16]. However, the converter loss, which may account over 50% of the total distribution power loss [17], has not been considered. Similar to the converter loss of DER systems in ac microgrids [18]–[21], the converter loss in dc microgrids can be calculated based on the quadratic function of the output currents as well [22]. In [17], [22], and [23], both the line loss and converter loss are taken into account as the distribution power loss of DER systems. However, these investigations are based on meshed dc microgrids and the controlled power loss is suboptimal. The distribution power loss can be further minimized by advanced modeling and control strategies.

For dc microgrids with parallel-connected DER systems, unlike the meshed dc networks, the output currents of DER systems can be directly used to calculate both the line loss and converter loss. Since the line loss and converter loss are quadratic functions of the output currents of DER systems, the distribution power loss of the parallel-connected DER systems is also a quadratic function of the output currents of DER systems, which can be proved as a convex function. Besides, by considering the current balance between the power supply and demand, the distribution power loss model can be further extended to be an equality-constrained convex function with respect to the current allocation coefficients of DER systems. Consequently, the distribution power loss can be reduced by optimizing the current allocation coefficients.

In this article, a Lagrange multiplier-based adaptive droop control is proposed to reduce both the line loss and the converter

Manuscript received September 8, 2020; revised December 1, 2020; accepted January 3, 2021. Date of publication January 12, 2021; date of current version May 5, 2021. Recommended for publication by Associate Editor D. Xu. *(Corresponding author: Yun Yang.)*

Yajie Jiang and Siew-Chong Tan are with the Department of Electrical and Electronic Engineering, The University of Hong Kong, 999077, Hong Kong (e-mail: u3005844@connect.hku.hk; sctan@eee.hku.hk).

Yun Yang is with the Department of Electrical Engineering, The Hong Kong Polytechnic University, 999077, Hong Kong, and also with the Department of Electrical and Electronic Engineering, The University of Hong Kong, 999077, Hong Kong (e-mail: yun1989.yang@polyu.edu.hk).

Shu-Yuen Ron Hui is with the Department of Electrical and Electronic Engineering, Nanyang Technological University, Singapore 639798, Singapore, and also with the Department of Electrical and Electronic Engineering, Imperial College London, SW7 2AZ London, U.K. (e-mail: ron.hui@ntu.edu.sg).

Color versions of one or more figures in this article are available at https://doi.org/10.1109/TPEL.2021.3050506.

Digital Object Identifier 10.1109/TPEL.2021.3050506

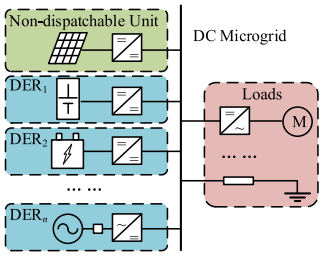

Fig. 1. Typical dc microgrid with *n* parallel-connected DER.

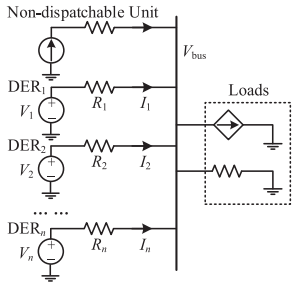

Fig. 2. Circuit diagram of dc microgrid.

loss of parallel-connected DER systems in dc microgrids. The proposed control is a three-layer hierarchical control that comprises a Lagrange multiplier method in the tertiary layer, an adaptive droop control in the secondary layer, and the conventional local dual-loop control in the primary layer. The Lagrange multiplier method of the tertiary layer is designed to provide the optimal current allocation coefficients for the adaptive droop control of the secondary layer by optimizing the distribution power loss model with equal constraints [24]. Based on the optimal current allocation coefficients and the total output current of the DER systems, the output current references of the DER systems can be calculated and tracked by the adaptive droop control to provide output voltage references of the DER systems for the local dual-loop control. Then, the duty ratios of the driving signals for the grid-connected converters are derived by the local dual-loop control based on the output voltage references. Obviously, the proposed control strategy is an online control scheme that can mitigate the distribution power loss of the DER systems in dc microgrids, while simultaneously regulating the output voltages and power within the tolerances. However, the proposed control scheme is only designed for parallel-connected DER systems. For distributed dc microgrids with meshed networks, further investigations are needed.

II. Distribution Power Loss Modeling of DER

The simplified architecture of a typical dc microgrid, which mainly comprises DER systems and loads, is shown in Fig. 1. The DER systems and loads are connected in parallel to the dc bus. In this article, DER refer to those dispatchable units that the power interactions between the units and microgrids can be regulated via grid-connected converters, such as energy storage systems, fuel cells, gas turbines, etc. Nondispatchable units, such as photovoltaic (PV) systems and wind energy conversion systems, are not considered as DER. Instead, they are be modeled as current sources [25]. The loads in dc microgrids may include constant power loads, constant resistive loads, nonlinear loads, variable loads, and pulse loads. Most loads require grid-connected converters to regulate the output power, voltage, or current. For instance, the output power of a motor driving system needs to be controlled at the rated power. However, some resistive loads, such as water heaters, can be directly connected to the dc microgrid without using grid-connected converters.

According to the simplified architecture in Fig. 1, the circuit diagram of a dc microgrid with *n* DERs can be depicted in Fig. 2.

Here, $V_{\rm bus}$ is the dc bus voltage. V_i and I_i ($i = 1, 2, \ldots, n$) are the output voltages and currents of DER. $I_i > 0$ indicates the current flowing from the *i*th DER to the dc bus and $I_i < 0$ indicates the current flowing from the dc bus to the *i*th DER. R_i ($i = 1, 2, \ldots, n$) are the distribution line resistances.

The distribution power loss of the DER includes the converter loss (i.e., $P_{\rm loss}^{\rm conv}$) of the grid-connected converters and the line loss (i.e., $P_{\rm loss}^{\rm line}$) on the distribution cables. The converter loss of the *i*th DER mainly comprises the average conduction loss of switches (i.e., $P_{{\rm conS}i}$), average conduction loss of bypass diodes (i.e., $P_{{\rm conD}i}$), average switching loss (i.e., $P_{{\rm sw}i}$), average reverse recovery loss of bypass diodes (i.e., $P_{{\rm rec}i}$), and power loss on resistive elements (i.e., $P_{{\rm res}i}$) as

$$P_{{\rm loss}i}^{\rm conv} = P_{{\rm conS}i} + P_{{\rm conD}i} + P_{{\rm sw}i} + P_{{\rm rec}i} + P_{{\rm res}i}. \tag{1a}$$

The power loss on the parasitic parameters and auxiliary circuits are generally negligible as compared to these power losses for the grid-connected converters in DER. In a system-level analysis of the grid-connected converters, based to the analysis in [17]–[22], [26], and [27], the converter loss of the *i*th DER can be simplified as a quadratic function of the output currents of DER as

$$P_{{\rm loss}i}^{\rm conv} = a_i I_i^2 + b_i |I_i| + c_i \tag{1b}$$

where $a_i > 0$, $b_i > 0$, and $c_i > 0$ are the conversion loss coefficients of the grid-connected converter of *i*th DER, which can be determined by identification methods (i.e., least square method, heuristic algorithm, neural networks, etc.) based on practical measurements [17], [18]. Besides, the line loss of the *i*th DER can be calculated based on

$$P_{{\rm loss}i}^{\rm line} = R_i I_i^2. \tag{2}$$

Based on (1a) and (2), the distribution power loss of the *i*th DER can be given as

$$P_{{\rm loss}i} = P_{{\rm loss}i}^{\rm conv} + P_{{\rm loss}i}^{\rm line} = (a_i + R_i) I_i^2 + b_i |I_i| + c_i. \tag{3a}$$

By defining the total output current of DER and the current allocation coefficient of the *i*th DER as $I_{\rm tol}$ and N_i, respectively, the distribution power loss of the *i*th DER can be further derived as

$$P_{{\rm loss}i} = (a_i + R_i)(N_i I_{\rm tol})^2 + b_i |N_i I_{\rm tol}| + c_i. \tag{3b}$$

Here, the total output current and the current allocation coefficient should satisfy

$$\sum_{i=1}^{n} N_i = 1 \tag{3c}$$

$$\sum_{i=1}^{n} I_i = I_{\text{tol}}. \tag{3d}$$

By defining $g(N_i) = \sum_{i=1}^{n} N_i - 1$, the constraint of the current allocation coefficient can be provided as

$$g(N_i) = 0. \tag{3e}$$

The total distribution power loss of all DER in the dc microgrid can be derived based on (3b), as

$$P_{\text{loss}}(N_i) = \sum_{i=1}^{n} P_{\text{loss}i} = \sum_{i=1}^{n} (a_i + R_i)(N_i I_{\text{tol}})^2 + b_i |N_i I_{\text{tol}}| + c_i. \tag{4}$$

According to (4), the total distribution power loss of DER can be regulated by current allocation coefficients N_i ($i = 1, 2, \ldots, n$).

By taking the first- and second-order partial derivatives of (4) with respect to N_i gives

$$\frac{\partial P_{\text{loss}}(N_i)}{\partial N_i} = 2N_i(a_i + R_i)(I_{\text{tol}})^2 + b_i |I_{\text{tol}}| \tag{5a}$$

$$\frac{\partial^2 P_{\text{loss}}(N_i)}{\partial N_i^2} = 2(a_i + R_i)(I_{\text{tol}})^2. \tag{5b}$$

Apparently, the first-order partial derivative of the power loss model is continuous and differentiable, and the Hessian of the power loss model is positive semidefinite for all N_i, which means the power loss model in (4) is strictly convex. Then, the distribution power loss of DER in the dc microgrid can be implemented by minimizing the power loss model with considerations of the equal constraint as

$$\begin{aligned} &\min \quad J = P_{\text{loss}}(N_i) \\ &\text{s.t.} \quad g(N_i) = 0. \end{aligned} \tag{6}$$

Compared to the objective function of the proposed method in (6), the objective function of the conventional method only comprises the line loss in (2). The analysis in [12], [17], and [22] reveal that the output voltages of the DER systems are required to be controlled in consensus (i.e., $V_1 = V_2 = \cdots = V_n$) by the conventional control to minimize the total line loss of the DER systems.

III. Proposed Control Strategy

The proposed control strategy consists of a Lagrange multiplier method to optimize the cost function in (6) and an adaptive droop control to regulate the output voltages of DER. A communication network is required to transfer data from the local sensors to the central controller to ensure the robustness of control in circumstances of plug-in and plug-off of DER systems, fluctuations of power sources and load variations, some parameter variations, etc. The flowchart of the control algorithm is depicted in Fig. 3. Optimal current allocation coefficients are provided by the Lagrange multiplier method to obtain the output voltage references of DER by the adaptive droop control. The output voltage references are further tracked by the conventional dual-loop control to regulate the duty ratios of the grid-connected converters. The output power of DER are strictly controlled within the tolerances by the Lagrange multiplier method as

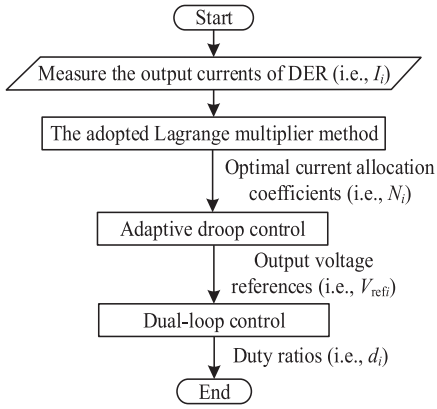

Fig. 3. Flowchart of the proposed control algorithm.

$$P_{\min i} \le P_i \le P_{\max i} \tag{7a}$$

where P_i is the output power of the ith DER. $P_{\min i}$ and $P_{\max i}$ are lower and upper bounds of the output power of the ith DER, respectively. Besides, the output voltages of DER are guaranteed to be controlled within the tolerances by the adaptive droop control as

$$V_{\min i} \le V_i \le V_{\max i} \tag{7.b}$$

where $V_{\min i}$ and $V_{\max i}$ are lower and upper bounds of the output voltage of the ith DER, respectively.

A. Adopted Lagrange Multiplier Method

Based on the cost function in (6), the Lagrange function of the Lagrange multiplier method can be defined as

$$\begin{aligned} L(N_i, \lambda) &= P_{\text{loss}}(N_i) + \lambda \cdot g(N_i) \\ &= \sum_{i=1}^{n} \left[(a_i + R_i)(N_i I_{\text{tol}})^2 + b_i N_i |I_{\text{tol}}| + c_i \right] \\ &\quad + \lambda \left(\sum_{i=1}^{n} N_i - 1 \right) \end{aligned} \tag{8}$$

where the Lagrange multiplier is nonzero (i.e., $\lambda \neq 0$). The optimal current allocation coefficients (i.e., N_i) can be derived by equating the first-order partial derivative of the Lagrange function to zero, as

$$\nabla_{N_i, \lambda} L(N_i, \lambda) = \left(\frac{\partial L}{\partial N_i}, \frac{\partial L}{\partial \lambda} \right) = 0 \tag{9}$$

which yields

$$N_i = -\frac{b_i\left|I_{\rm tol}\right|+\lambda}{2(a_i+R_i)(I_{\rm tol})^2} \tag{10a}$$

$$\lambda = -\frac{\sum_{i=1}^{n}\frac{b_i}{2(a_i+R_i)|I_{\rm tol}|}+1}{\sum_{i=1}^{n}\frac{1}{2(a_i+R_i)(I_{\rm tol})^2}}. \tag{10b}$$

However, the derived N_i in (10a) may not be eventually adopted, since the output power of some DER with the derived N_i in (10a) may violate the constraint in (7a). Therefore, maximum and minimum output power of DER (i.e., $P_{i\cdot\max}$ and $P_{i\cdot\min}$) are required to be further determined. The output power of each DER can be estimated by adding the distribution power loss and the injected power from each DER to the dc bus (i.e., $P_i = P_{{\rm loss}i}+P_{{\rm s2b}i}$). Based on (10a) and the total output current of DER, the output current of each DER can be calculated using $|I_i| = |N_i I_{\rm tol}|$. Then, the distribution power loss of each DER can be obtained based on (3a). Besides, the injected power from each DER to the dc bus can be calculated by multiplying the dc bus voltage and the output current of each DER (i.e., $P_{{\rm s2b}i} = V_{\rm bus}|I_i|$). As the dc bus voltage can be controlled within the tolerances in (7b), the maximum and minimum injected power are $P_{{\rm s2b}i\_\max} = V_{\max i}|I_i|$ and $P_{{\rm s2b}i\_\min} = V_{\min i}|I_i|$, respectively. Hence, the maximum and minimum output power of each DER can be calculated by $P_{i\_\max} = P_{{\rm loss}i}+P_{{\rm s2b}i\_\max}$ and $P_{i\_\min} = P_{{\rm loss}i}+P_{{\rm s2b}i\_\min}$, respectively. If the maximum output power of the DER is larger than the upper bound (i.e., $P_{i\_\max} > P_{\max i}$), the output power of the DER is required to be regulated at the upper bound by controlling the output current of the DER as

$$|I_{\max i}| = \frac{\sqrt{(b_i+V_{\max i})^2+4(a_i+R_i)(P_{\max i}-c_i)}}{2(a_i+R_i)}. \tag{11a}$$

Conversely, if the minimum output power of the DER is smaller than the lower bound (i.e., $P_{i\_\min} > P_{\min i}$), the output power of the DER is required to be regulated at the lower bound by controlling the output current of the DER as

$$|I_{\min i}| = \frac{\sqrt{(b_i+V_{\min i})^2+4(a_i+R_i)(P_{\min i}-c_i)}}{2(a_i+R_i)}. \tag{11b}$$

When the output power of the ith DER is regulated at the upper bound (or the lower bound), the total output current of the remaining DER is $|I'_{\rm tol}| = |I_{\rm tol}| - |I_{\max i}|$ (or $|I'_{\rm tol}| = |I_{\rm tol}| - |I_{\min i}|$). According to (5a) and (5b), the distribution power loss function of the remaining DER systems still remains convex. Thus, by combing (10a), (11a), and (11b), the optimal current allocation coefficients derived by the adopted Lagrange multiplier method can be given as

$$N_i = \begin{cases} \frac{|I_{\max i}|}{|I_{\rm tol}|} & P_i > P_{\max i} \\ \frac{|I_{\min i}|}{|I_{\rm tol}|} & P_i < P_{\min i} \\ -\frac{b_i|I_{\rm tol}|+\lambda}{2(a_i+R_i)(I_{\rm tol})^2} & P_{\min i} \le P_i \le P_{\max i}. \end{cases} \tag{12}$$

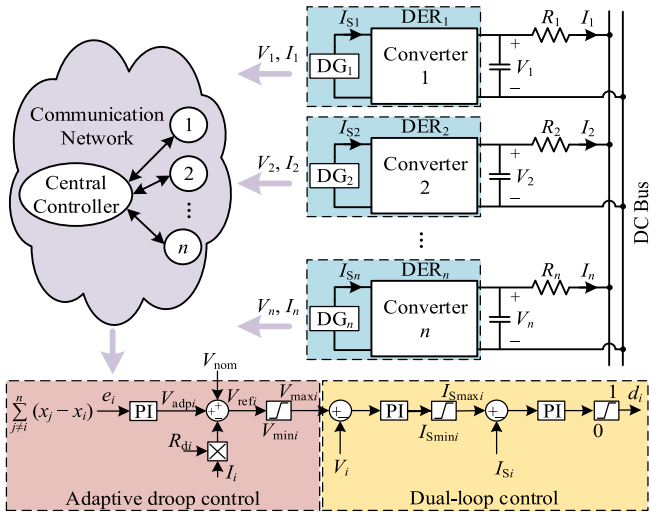

Fig. 4. Schematic diagram of the adaptive droop control and dual-loop control.

B. Adaptive Droop Control

The adaptive droop control is designed to track the output currents of DER accurately even if the power conditions of the system change (e.g., plug-in/off of RES systems, fluctuations of power sources and load variations). The control block diagram of the adaptive droop control is shown in Fig. 4. The adaptive droop control provides the output voltage references of DER (i.e., $V_{{\rm ref}i}$) for the conventional dual-loop control.

The control variables of the adaptive droop control are defined as $x_i = \frac{I_i}{N_i}$, where I_i are measured by current sensors and N_i are provided by the Lagrange multiplier method based on (12). Then, the total current allocation errors of the system can be written as

$$e_i = \sum_{i=1,j\neq i}^{n}(x_j - x_i) \tag{13}$$

which needs to be controlled at zero such that the control variables (i.e., x_i) are equalized for all the DER system as

$$\frac{I_1}{N_1} = \frac{I_2}{N_2} = \cdots = \frac{I_n}{N_n}. \tag{14}$$

The total current allocation errors are compensated by conventional proportional-integral (PI) controllers to derive adaptive voltage terms (i.e., $V_{{\rm adp}i}$) for the output voltage references of DER systems, as

$$V_{{\rm adp}i} = \left(k_{{\rm P}i} + \frac{k_{{\rm I}i}}{s}\right)e_i \tag{15}$$

where $k_{{\rm P}i}$ and $k_{{\rm I}i}$ are the proportional and integral gains of the ith PI controller (i.e., $k_{{\rm P}i} > 0$ and $k_{{\rm I}i} > 0$), respectively. By substituting (13) into (15)

$$V_{{\rm adp}i} = k_{{\rm P}i}\sum_{i=1,j\neq i}^{n}(x_j - x_i) + \frac{k_{{\rm I}i}}{s}\sum_{i=1,j\neq i}^{n}(x_j - x_i). \tag{16}$$

Then, the output voltage references (i.e., $V_{\mathrm{ref}i}$) can be provided by the droop control as

$$V_{\mathrm{ref}i} = V_{\mathrm{nom}} - R_{\mathrm{d}i} I_i + V_{\mathrm{adp}i} \tag{17}$$

where V_{nom} is the nominal dc bus voltage and $R_{\mathrm{d}i}$ is the droop coefficient of the *i*th DER. A voltage limiter is adopted in the droop control to ensure the output voltage references are within the tolerances, as given in (7b). According to (16) and (17), when the control variable of the *i*th DER (i.e., x_i) is increased, the output voltage reference of the *i*th DER (i.e., $V_{\mathrm{ref}i}$) will be decreased. Consequently, the output current of the *i*th DER (i.e., I_i) will decrease such that the control variable of the *i*th DER (i.e., x_i) will decrease. Conversely, when the control variable of the *i*th DER (i.e., x_i) is decreased, the output voltage reference of the *i*th DER (i.e., $V_{\mathrm{ref}i}$) will be increased. As a result, the output current of the *i*th DER (i.e., I_i) will increase such that the control variable of the *i*th DER (i.e., x_i) will increase. Obviously, the adopted adaptive droop control can effectively regulate the total current allocation errors to be zero. The robustness of the adopted adaptive droop control is better than that of the conventional adaptive droop control by introducing the adaptive voltage term $V_{\mathrm{adp}i}$.

Based on (16), the Laplace transformation of the adaptive voltages for all DER can be derived as

$$\begin{aligned} s\mathbf{V}_{\mathrm{adp}}(s) &= \mathbf{G}(s)(\mathbf{E}-n\mathbf{I})\mathbf{x}(s) \\ &= s\mathbf{k_P}(\mathbf{E}-n\mathbf{I})\mathbf{x}(s) + \mathbf{k_I}(\mathbf{E}-n\mathbf{I})\mathbf{x}(s) \end{aligned} \tag{18}$$

where $\mathbf{V}_{\mathrm{adp}}(s) = [V_{\mathrm{adp1}}(s), \ldots, V_{\mathrm{adpn}}(s)]^T$, $\mathbf{x}(s) = [x_1(s), \ldots, x_n(s)]^T$, $\mathbf{G}(s) = \mathrm{diag}\{sk_{\mathrm{P1}} + k_{\mathrm{I1}}, \ldots, sk_{\mathrm{Pn}} + k_{\mathrm{In}}\}$, $\mathbf{k_P} = \mathrm{diag}\{k_{\mathrm{P1}}, \ldots, k_{\mathrm{Pn}}\}$, $\mathbf{k_I} = \mathrm{diag}\{k_{\mathrm{I1}}, \ldots, k_{\mathrm{In}}\}$, $\mathbf{I}$ is an n×n identity matrix and $\mathbf{E}$ is an n×n matrix with all the elements being one. When the system reaches the steady state (i.e., $t \to \infty$), based on the final value theorem (i.e., $s = 0$)

$$\lim_{s\to 0} (\mathbf{E}-n\mathbf{I})\mathbf{x}(s) = 0. \tag{19}$$

By rewriting (19)

$$\begin{bmatrix} \sum_{i=1}^{n}(x_i - x_1) & \sum_{i=1}^{n}(x_i - x_2) \cdots \sum_{i=1}^{n}(x_i - x_n) \end{bmatrix}^{\mathbf{T}} = [0 \quad 0 \quad \cdots \quad 0]^{\mathbf{T}}. \tag{20}$$

According to the Theorem 1 in the appendix, the control variables (i.e., x_1, x_2, …, x_n) are converged to a consensus at steady state as

$$x_1 = x_2 = \cdots = x_n. \tag{21}$$

It is worth noting that the convergence of the control variables can still hold by even considering communication delays in the emerging dc microgrids with relatively short geographical distances and advanced communication technology [28].

According to the analysis in [29] and [30], the adaptive voltage term (i.e., $V_{\mathrm{adp}i}$) in the time domain (i.e., $v_{\mathrm{adp}i}(t)$) can be further derived by considering the non-negligible communication delay as

$$\begin{aligned} v_{\mathrm{adp}i}(t) = k_{\mathrm{P}i} \sum_{i=1, j\neq i}^{n} [x_j(t-\tau_j) - x_i(t)] \\ + k_{\mathrm{I}i} \int \sum_{i=1, j\neq i}^{n} [x_j(t-\tau_j) - x_i(t)]dt. \end{aligned} \tag{22}$$

Because the state variables are generally invariant during the communication delay period, by taking the derivatives on both sides of (22)

$$\dot{v}_{\mathrm{adp}i}(t) = k_{\mathrm{I}i} \sum_{i=1, j\neq i}^{n} [x_j(t-\tau_j) - x_i(t)] \tag{23}$$

where τ_j denotes the communication delay between the node *j* and the node *i*. Here, the state variables satisfy

$$x_i(t) = G_i v_{\mathrm{adp}i}(t) \tag{24}$$

where the line admittance G_i is generally constant during the communication delay period and $G_i > 0$. Besides, by defining the error between each state variable and the reference as

$$\varepsilon_i(t) = x_i(t) - x_{\mathrm{ref}}. \tag{25}$$

The dynamics can be further derived by substituting (24) into (25) as

$$\dot{\varepsilon}_i(t) = G_i \dot{v}_{\mathrm{adp}i}(t). \tag{26}$$

By substituting (23) into (26) to eliminate the term $\dot{v}_{\mathrm{adp}i}(t)$

$$\dot{\varepsilon}_i(t) = G_i k_{\mathrm{I}i} \sum_{i=1, j\neq i}^{n} [x_j(t-\tau_j) - x_i(t)]. \tag{27}$$

According to (25) and (27), the candidate Lyapunov–Krasovskii function can be designed as [30]

$$V(t) = \sum_{i=1}^{n} [\varepsilon_i(t)]^2 + \sum_{i=1}^{n} \sum_{j\neq i} G_i k_{Ii} \int_{t-\tau_j}^{t} [\varepsilon_j(\sigma)]^2 d\sigma. \tag{28}$$

It is obvious that $V(t) \geq 0$ can always hold. Based on (28), the derivative of the Lyapunov–Krasovskii function can be derived as

$$\begin{aligned} \dot{V}(t) = 2\sum_{i=1}^{n} \varepsilon_i(t)\dot{\varepsilon}_i(t) \\ + \sum_{i=1}^{n} \sum_{j\neq i} G_i k_{Ii} \{[\varepsilon_j(t)]^2 - [\varepsilon_j(t-\tau_j)]^2\}. \end{aligned} \tag{29}$$

By substituting (27) into (29) to eliminate the term $\dot{\varepsilon}_i(t)$

$$\begin{aligned} \dot{V}(t) = 2\sum_{i=1}^{n} \sum_{j\neq i} G_i k_{Ii} \varepsilon_i(t)[\varepsilon_j(t-\tau_j) - \varepsilon_i(t)] \\ + \sum_{i=1}^{n} \sum_{j\neq i} G_i k_{Ii} \{[\varepsilon_j(t)]^2 - [\varepsilon_j(t-\tau_j)]^2\}. \end{aligned} \tag{30}$$

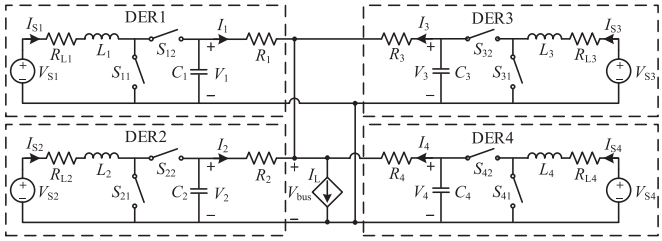

Fig. 5. Circuitry of the dc microgrid with four parallel-connected DER systems in simulation.

Since the communication graph of the adopted communication graph is naturally balanced

$$\sum_{i=1}^{n}\sum_{j\neq i}\varepsilon_i(t)^2 = \sum_{i=1}^{n}\sum_{j\neq i}\varepsilon_j(t)^2. \tag{31}$$

By substituting (31) into (30) to eliminate the term $\sum_{i=1}^{n}\sum_{j\neq i}\varepsilon_j(t)^2$

$$\dot{V}(t) = -\sum_{i=1}^{n}\sum_{j\neq i} G_i k_{Ii}[\varepsilon_i(t) - \varepsilon_j(t-\tau_j)]^2. \tag{32}$$

Obviously, the Lyapunov stability is guaranteed (i.e., $\dot{V}(t) \leq 0$). The Lyapunov–Krasovskii function (i.e., $V(t)$) converges to zero asymptotically. Accordingly, the state variables (i.e., $x_i(t)$) can converge to the reference (i.e., $x_{\rm ref}$) asymptotically. Therefore, the proposed control strategy is validated to achieve proportional current allocations even with the considerations of non-negligible communication delays.

The derived output voltage references by the adaptive droop control are further tracked by the dual-loop control to regulate the grid-connected converters. The source currents (i.e., $I_{{\rm S}i}$) and the duty ratios of grid-connected converters (i.e., d_i) are strictly controlled within the tolerances (i.e., $I_{{\rm S}\min i} \leq I_{{\rm S}i} \leq I_{{\rm S}\max i}$ and $0 \leq d_i \leq 1$) by PI controllers. It is worth noting that the proposed control strategy is also validated for the grid-connected converters with other types of local control (e.g., one-loop voltage control).

IV. Simulation Results

Simulation-based case studies are carried out in MATLAB/Simulink based on a 48 V dc microgrid with four DER systems being connected in parallel to a dc bus. The circuitry of the dc microgrid in simulation is depicted in Fig. 5. Nonisolated boost converters are adopted as the grid-connected converters for the DER systems. Without losing the generality, nondispatchable units and loads are modeled as a current sink, the current of which equals to the total output current of the DER systems to ensure the current balance in the dc microgrid. Hence, the current sink is positive when the total output current of the DER systems is negative. Conversely, the current sink is negative when the total output current of the DER systems is positive. The main specifications of the dc microgrid are listed in Table I. The parameters of the four DER systems are identical (i.e., $L_1 = L_2 = L_3 = L_4$, $C_1 = C_2 = C_3 = C_4$, and $R_{\rm L1} = R_{\rm L2} = R_{\rm L3} = R_{\rm L4}$, etc.), while the line resistances of the four DER systems are different. It should be noted that the DER systems with different time constants will not affect the control performance since the operating frequency of the local dual-loop control is much faster than that of the higher layer control [31], [32]. The dc bus voltage is allowed to deviate within 5% (i.e., $V_{\min} = 45.6$ V and $V_{\max} = 50.4$ V). The rated, minimum, and maximum power of the four DER systems are 300 W, 0 W, and 350 W, respectively (i.e., $P_{\min} = 0$ W and $P_{\max} = 350$ W). The switching frequency of the grid-connected converters is 100 kHz. The communication delay is set to be 0.01 s.

TABLE I
Main Specificaitons of DC Microgrid in Simulation

Descriptions	Symbol	Value
Nominal DC bus voltage	$V_{\rm bus\_nom}$	48 V
Lower limit of the DC bus voltage	$V_{\min}$	45.6 V
Upper limit of the DC bus voltage	$V_{\max}$	50.4 V
Rated power of the DER systems	$P_{\rm rate}$	300 W
Lower power limit of the DER systems	$P_{\min}$	0 W
Upper power limit of the DER systems	$P_{\max}$	350 W
Rate voltages of the distributed generations	$V_{{\rm S}i\_{\rm rated}}$	24 V
Inductances of the converter	L_i	460 μH
ESR of the inductances	$R_{{\rm L}i}$	0.1 Ω
Output capacitances of the converter	C_i	10.1 μF
Forward voltages of the bypass diodes	$V_{{\rm D}i}$	0.3 V
Output capacitances of the switches	C_{si}	102 pF
ON resistances of the switches	R_{si}	72 mΩ
Line resistance of DER1	R_1	0.5 Ω
Line resistance of DER2	R_2	0.8 Ω
Line resistance of DER3	R_3	0.2 Ω
Line resistance of DER4	R_4	1.1 Ω

The parameters of the controllers in simulation are provided in Table II. The parameters of the PI compensators in both the adaptive droop control and the conventional dual-loop control are identical for all the four DER (i.e., $K_{\rm P1} = K_{\rm P2} = K_{\rm P3} = K_{\rm P4}$, $K_{\rm I1} = K_{\rm I2} = K_{\rm I3} = K_{\rm I4}$, $K_{\rm P11} = K_{\rm P12} = K_{\rm P13} = K_{\rm P14}$, $K_{\rm I11} = K_{\rm I12} = K_{\rm I13} = K_{\rm I14}$, $K_{\rm P21} = K_{\rm P22} = K_{\rm P23} = K_{\rm P24}$, and $K_{\rm I21} = K_{\rm I22} = K_{\rm I23} = K_{\rm I24}$). The droop coefficients of the adaptive droop control are also the same for all the four DER (i.e., $R_{\rm d1} = R_{\rm d2} = R_{\rm d3} = R_{\rm d4}$). The sampling frequency of the controllers is 100 kHz.

A. Convexity of the Distribution Power Loss Model

The convexity of the derived distribution power loss model in (4) is initially verified by the simulation. For the dc microgrid with two DER (i.e., DER1 and DER2, DER1 and DER3, DER1 and DER4, DER2 and DER3, DER2 and DER4, and DER3 and DER4), the distribution power loss of the DER systems (i.e., $P_{\rm loss}$) versus different values of current allocation coefficients (i.e., N_1, N_2, and N_3) are plotted in Fig. 6. The sum of the current allocation coefficients for each case is 1. Apparently, the distribution power loss curve is convex with only one minimum point regardless of different total output currents of the DER systems (i.e., $I_{\rm tol} = 12$ A, $I_{\rm tol} = 16$ A, and $I_{\rm tol} = 20$ A). The coordinates of the minimum points are labeled in Fig. 6.

TABLE II
PARAMETERS OF CONTROLLERS IN SIMULATION

Descriptions	Symbol	Value
Proportional gain of the PI compensation in the adaptive droop control	K_{Pi}	0.02
Integral gain of the PI compensation in the adaptive droop control	K_{Ii}	1
Proportional gain of the PI voltage compensation in the dual-loop control	K_{P1i}	20
Integral gain of the PI voltage compensation in the dual-loop control	K_{I1i}	10
Proportional gain of the current PI current compensation in the dual-loop control	K_{P2i}	100
Integral gain of the PI current compensation in the dual-loop control	K_{I2i}	20
Lower bound of the output voltage of DER	V_{mini}	45.6 V
Upper bound of the output voltage of DER	V_{maxi}	50.4 V
Lower bound of the source current of DER	I_{Smini}	0 A
Upper bound of the source current of DER	I_{Smaxi}	15 A
Droop coefficient	R_{di}	0.05 Ω
Converter loss coefficients of DER1	a	1.166
	b	2.410
	c	1.110
Converter loss coefficients of DER2	a	0.176
	b	1.040
	c	2.040
Converter loss coefficients of DER3	a	0.477
	b	0.956
	c	1.360
Converter loss coefficients of DER4	a	0.730
	b	1.600
	c	0.600

For the dc microgrid with three DER (i.e., DER1, DER2, and DER3, DER1, DER 2, and DER4, and DER2, DER3, and DER4), the distribution power loss of the DER systems versus different values of current allocation coefficients are plotted in Fig. 7. The total output current of the three DER systems is 16 A and the sum of the current allocation coefficients for each case is 1. Obviously, the distribution power loss surfaces are convex with only one minimum point in each case. The minimum distribution power loss are 107.5, 146.4, 123.2, and 106 W, respectively.

Similarly, the distribution power loss of the DER systems versus different values of current allocation coefficients in a dc microgrid with four DER are presented in Fig. 8. The total output current of the four DER systems is 16 A and the sum of the current allocation coefficients is 1. In Fig. 8(a)–(d), one current allocation coefficient is fixed at 0.1, such that the constraint in (7a) is not violated. Apparently, the distribution power loss surfaces are convex and the minimum power loss are 115.3, 129.4, 152.1, and 115.3 W, respectively. In Fig. 8(e)–(h), the current allocation coefficients are fixed at 0.3118, 0.337, 0.348, and 0.3117, respectively [i.e., $N_1 = 0.3118$ in Fig. 8(e), $N_2 = 0.337$ in Fig. 8(f), $N_3 = 0.348$ in Fig. 8(g), and $N_4 = 0.3117$ in Fig. 8(h)], such that the output power of DER are limited at the maximum power. Nevertheless, the distribution power loss surfaces are still convex, which is in good agreement with theoretical analysis. The minimum power loss are 135.1, 119.6, 119.2, and 136.8 W, respectively. For the output power of DER

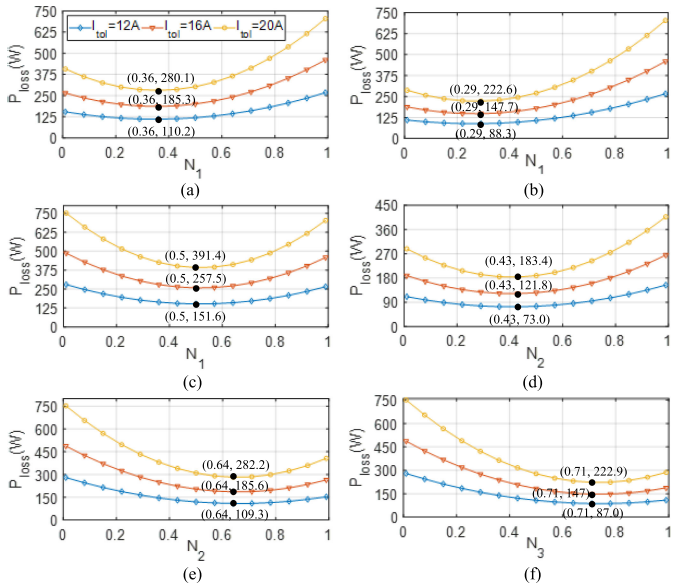

Fig. 6. Distribution power loss versus current allocation coefficients for the dc microgrid with two DER systems. (a) DER_1 and DER_2. (b) DER_1 and DER_3. (c) DER_1 and DER_4. (d) DER_2 and DER_3. (e) DER_2 and DER_4. (f) DER_3 and DER_4.

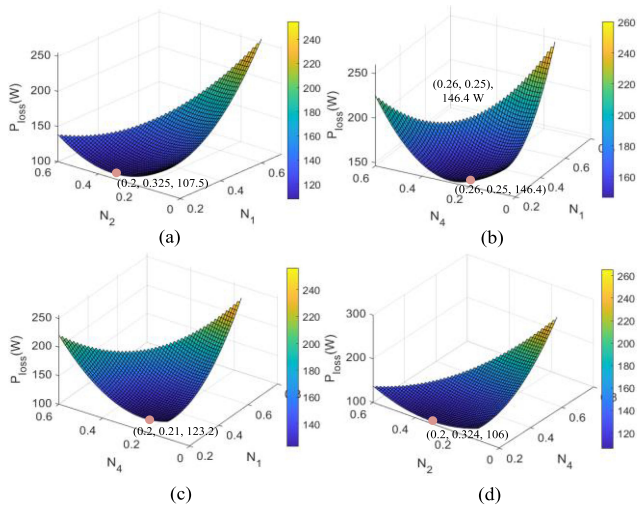

Fig. 7. Distribution power loss versus current allocation coefficients for the dc microgrid with three DER systems. (a) DER_1, DER_2, and DER_3. (b) DER_1, DER_2, and DER_4. (c) DER_1, DER_3, and DER_4. (d) DER_2, DER_3, and DER_4.

are limited at the minimum power, one current allocation coefficient is fixed at 0. Therefore, the distribution power loss surfaces are the same as the power loss surfaces of the dc microgrid with three DER in Fig. 7. The surfaces are also verified to be convex.

B. Validation of the Proposed Control Strategy

In simulation, three cases are investigated to verify the effectiveness of the proposed control strategy to mitigate more distribution power loss than the conventional control strategy for the dc microgrid with four DER systems. Details of the three case studies are provided in Table III. In case 1, the output power of DER systems (i.e., P) being controlled by the proposed control

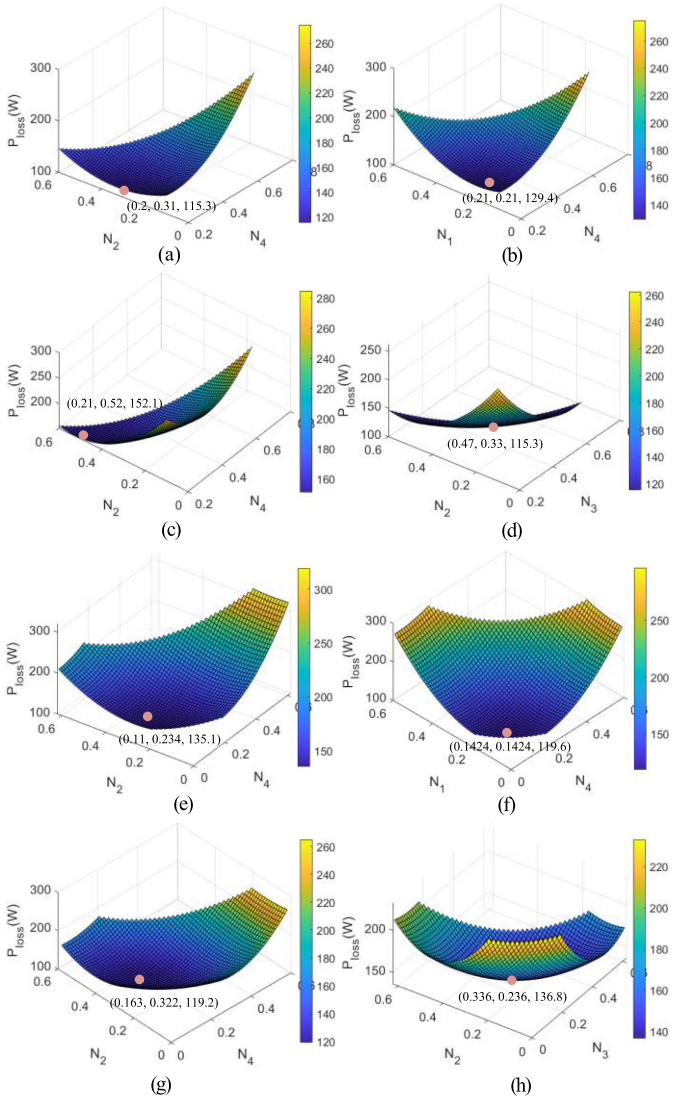

Fig. 8. Distribution power loss versus current allocation coefficients for the dc microgrid with four DER systems. (a) $N_1 = 0.1$. (b) $N_2 = 0.1$. (c) $N_3 = 0.1$. (d) $N_4 = 0.1$. (e) $N_1 = 0.3118$. (f) $N_2 = 0.337$. (g) $N_3 = 0.348$. (h) $N_4 = 0.3117$.

TABLE III
DETAILS OF THE CASE STUDIES IN SIMULATION

Case		Descriptions	
1	1.1	Output power of DER systems are within the bounds	positive
	1.2		negative
2		Output power of one DER system is clamped at the boundary	
3		Different numbers of DER systems in the DC microgrid	
4		Practical power supply and demand of DER systems in a day	

strategy are within the boundaries. The output power of the DER system is positive when it flows from the DER system to the dc bus, as presented in case 1.1. Conversely, the output power of the DER system is negative when it flows from the dc bus to the DER system, as presented in case 1.2. In case 2, the output powers of one DER system controlled by the conventional control strategy and the proposed control strategy without considering the power constraint in (7a) are beyond the power limit. But the output

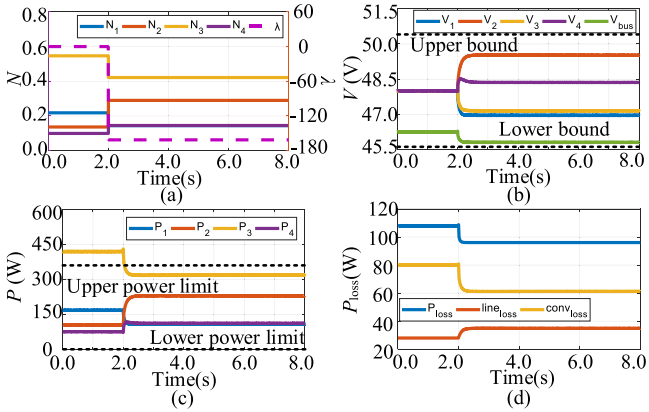

Fig. 9. Waveforms of the (a) current allocation coefficients and Lagrange multiplier, (b) output voltages of DER, (c) output power of DER, and (d) distribution power loss for the case 1.1.

power of the DER system controlled by the proposed control strategy with the power constraint is clamped at the boundary. In case 3, other than the four DER systems, three and five DER systems controlled by the conventional control strategy and the proposed control strategy are also investigated. In case 4, a daylong variable power supply by a nondispatchable unit and a power demand by the loads are adopted for the dc microgrid with four DER systems.

Fig. 9 shows the waveforms of the current allocation coefficients, Lagrange multiplier, output voltages and power of the DER systems, bus voltage, and distribution power loss of the dc microgrid controlled by the conventional control strategy and the proposed control strategy for case 1.1. The total output current of the DER systems is 13 A and the current sink is modeled to be 13 A. The conventional control strategy is adopted to reduce the line loss of the DER systems during the period from 0 to 2 s whereas the proposed control strategy is adopted to mitigate the distribution power loss of the DER systems during the period from 2 to 8 s. For the conventional control strategy, since the Lagrange multiplier method is not included, the Lagrange multiplier (i.e., λ) is 0. The output voltages of the DER systems are converged at 48 V and the bus voltage is at 46.25 V. The output power of the DER3 is 419 W, which is beyond the upper limit of 350 W. The line loss is minimized at 29 W, while the conversion loss and total distribution power loss are 80 W and 109 W, respectively. However, for the proposed control strategy, the Lagrange multiplier is calculated to be –162.4 and the current allocation coefficients are controlled at $N_1 = 0.144$, $N_2 = 0.2896$, $N_3 = 0.4214$, and $N_4 = 0.1449$, respectively. As a result, the output voltages and power of the DER systems are within the boundaries. Compared to the conventional control strategy, the line loss of the proposed control strategy is increased (i.e., 34.9 W $>$ 29 W), the total distribution power loss is mitigated (i.e., 96.1 W $<$ 109 W) since the conversion loss is significantly reduced from 80 to 61.2 W. The total distribution power loss is reduced by about 11.83%. To validate the effectiveness of the proposed control with non-negligible communication delay, the communication delay is changed from 0.01 to 0.05 s and 0.1 s. The corresponding waveforms of the distribution power loss are

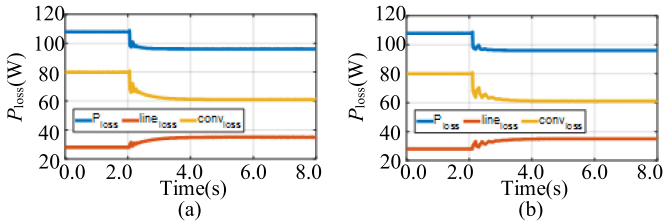

Fig. 10. Waveforms of the distribution power loss with communication delay of (a) 0.05 s and (b) 0.1 s for the case 1.1.

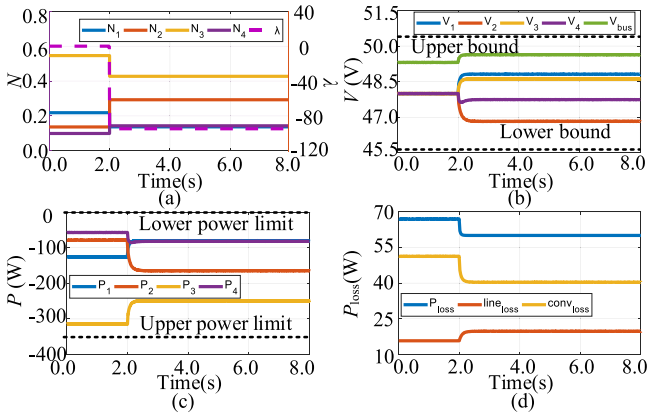

Fig. 11. Waveforms of the (a) current allocation coefficients and Lagrange multiplier, (b) output voltages of DER, (c) output power of DER, and (d) distribution power loss for the case 1.2.

plotted in Fig. 10. Apparently, the existence of non-negligible communication delay will not affect the reduced power loss at steady states. Although the dynamic performances are deteriorated, the power curves can eventually converge asymptotically, which validates the aforementioned analysis.

Similar to the case 1.1, the waveforms of current allocation coefficients, Lagrange multiplier, output voltages and power of the DER systems, bus voltage, and distribution power loss of the dc microgrid controlled by the conventional control strategy and the proposed control strategy for case 1.2 are presented in Fig. 11. However, the total output current of the DER systems is 12 A and the current sink is modeled to be –12 A. For case 1.2, the Lagrange multiplier of the proposed control strategy is calculated to be –94.72 and the corresponding current allocation coefficients are $N_1 = 0.1371$, $N_2 = 0.2926$, $N_3 = 0.427$, and $N_4 = 0.1433$, respectively. The corresponding output voltages and power of the DER systems are well controlled within the boundaries. The comparisons of the distribution power loss between the two control strategies are exhibited in Fig. 11(d). The total distribution power loss is reduced by about 10.3% (from 67 to 60.1 W) by the proposed control strategy.

In case 2, the conventional control strategy is adopted during the period from 0 to 2 s, whereas the proposed control strategy without considering the output power constraint in (7a) is adopted during the period from 2 to 6 s and with the consideration of the output power constraint in (7a) is used during the period from 6 to 10 s. The total output current of the DER systems is 18 A and the current sink is modeled to be

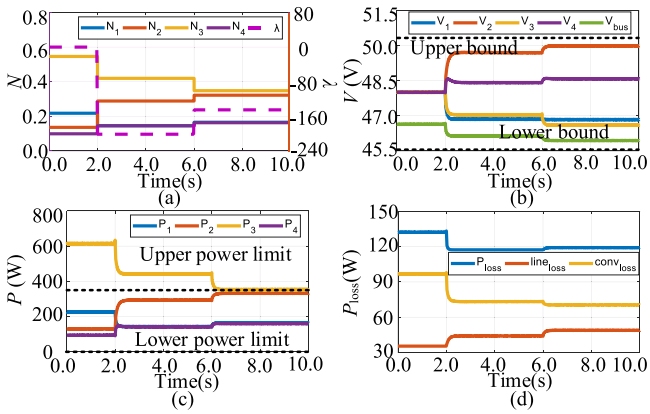

Fig. 12. Waveforms of the (a) current allocation coefficients and Lagrange multiplier, (b) output voltages of DER, (c) output power of DER, and (d) distribution power loss for the case 2.

18 A. The Lagrange multiplier is changed from 0 to –201.3 to –145. The corresponding current allocation coefficients of the proposed control strategy without the power constraint are $N_1 = 0.1463$, $N_2 = 0.2887$, $N_3 = 0.4196$, and $N_4 = 0.1455$, while the current allocation coefficients of the proposed control strategy with the power constraint are $N_1 = 0.1661$, $N_2 = 0.3222$, $N_3 = 0.3485$, and $N_4 = 0.1633$, as shown in Fig. 12(a). Although all the bus voltages are controlled within the limits, the output powers of DER3 controlled by the conventional control strategy and the proposed control strategy without considering the power constraint in (7a) (i.e., 441.3 and 349.9 W) are beyond the upper power limit (i.e., 350 W). But the output power of the DER3 controlled by the proposed control strategy with the constraint in (7a) is clamped at the boundary of 350 W, as shown in Fig. 12(c). Therefore, both the conventional control strategy and the proposed control strategy without considering the power constraint cannot meet the requirement. The proposed control strategy with the power constraint can reduce the distribution power loss by about 9.83% as compared to the conventional control strategy (i.e., from 132. 2 to 119.2 W).

In case 3, the four DER systems (i.e., DER1, DER2, DER3, and DER4) are connected to the dc bus during the period from 0 to 4 s. At 4 s, the DER4 is disconnected from the dc bus. Hence, three DER systems (i.e., DER1, DER2, and DER3) are connected to the dc bus during the period from 4 to 12 s. At 12 s, two additional DER systems (i.e., DER4 and DER5) are connected to the dc bus. Thus, five DER systems are connected to the dc bus during the period from 12 to 20 s. The parameters of the DER5 are identical to those of the DER3. The total output current of the DER systems is 13 A and the current sink is modeled to be 13 A. The conventional control strategy is adopted during the periods from 0 to 2 s, 8 to 12 s, and 16 to 20 s, while the proposed control strategy is applied during the periods from 2 to 4 s, 4 to 8 s, and 12 to 16 s. The corresponding Lagrange multipliers of the proposed control strategy are –109.7, –228, and –88.6, respectively, as shown in Fig. 13(a). The output voltages and power of the DER systems are well controlled within tolerances by the proposed control strategy, as shown in Fig. 13(b). The total distribution power loss are 78.3, 71.5,

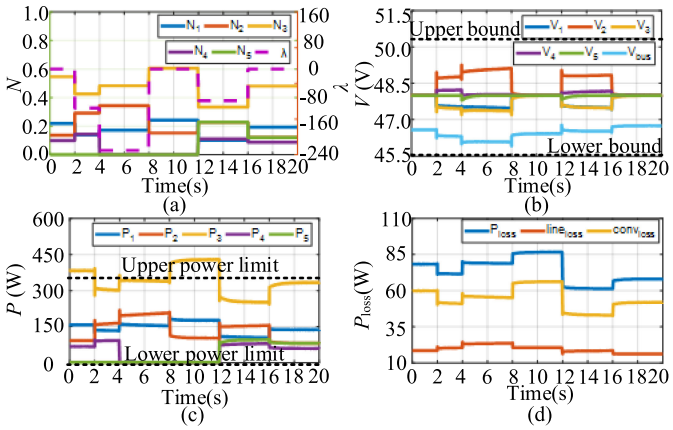

Fig. 13. Waveforms of the (a) current allocation coefficients and Lagrange multiplier, (b) output voltages of DER, (c) output power of DER, and (d) distribution power loss for the case 3.

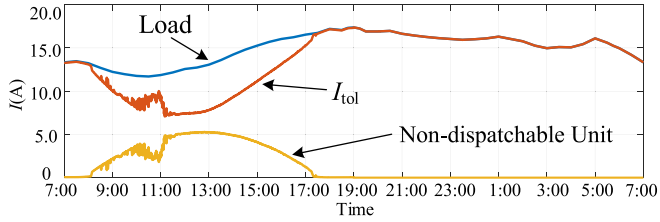

Fig. 14. Output currents of the nondispatchable unit, DER systems, and load in case 4.

78.8, 86.7, 61.4, and 68.2 W for each time period, as shown in Fig. 13(c). Compared to the conventional control strategy, the proposed control strategy can reduce the distribution power loss about 8.68% for the four DER systems, 9.11% for the three DER systems, and 9.97% for the five DER systems. The scalability of the proposed control strategy for different numbers of DER systems being plug-and-played in the dc microgrid is validated.

In case 4, a nondispatchable unit (i.e., a PV system) is connected to the dc microgrid with four DER systems. The daylong output currents of the nondispatchable unit, DER systems, and load are plotted in Fig. 14. The variable output currents of the nondispatchable unit and load are provided based on the measurements in practice [33], [34]. The current difference between the nondispatchable unit and load are compensated by the total output current of the DER systems (i.e., $I_{\rm tol}$). Fig. 15 show the waveforms of current allocation coefficients, Lagrange multiplier, output voltages and power of the DER systems, bus voltage, and distribution power loss of the dc microgrid being controlled by the conventional control strategy and the proposed control strategy. Obviously, the output voltages and power of the DER systems are controlled within the constraints. The comparisons of the total distribution power loss between the conventional control strategy and the proposed control strategy are presented in Fig. 15(d). The distribution power loss is reduced by the proposed control strategy. By accumulating the distribution power loss, the distribution energy loss of the dc microgrid with four DER systems in one day can be 2.058 and 1.835 kWh by the conventional control strategy and proposed

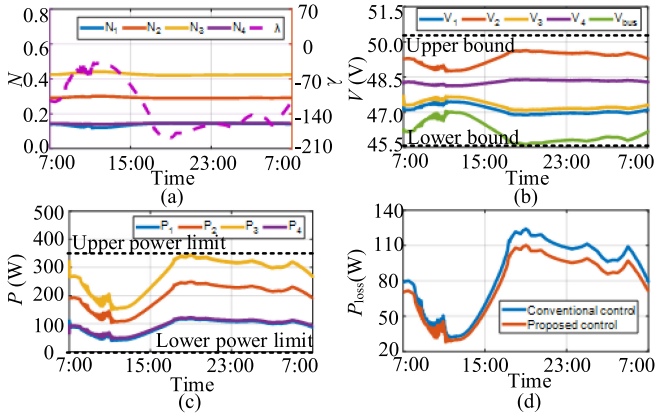

Fig. 15. Waveforms of the (a) current allocation coefficients and Lagrange multiplier, (b) output voltages of DER, (c) output power of DER, and (d) distribution power loss for the case 4.

control strategy, respectively. The loss reduction by the proposed control strategy is about 10.84%.

V. Experimental Verifications

Experiments are conducted on a 48 V dc microgrid with two/three DER systems being connected in parallel to the dc bus via nonisolated boost converters. The photograph of the test bench is presented in Fig. 16(a). The main parameters of the grid-connected boost converters are identical to the parameters provided in Table I. The rated voltages of the distributed generations are 38 V for all the DER systems. The current sink in the dc microgrid is implemented by the electronic load PLA5K-800-100E. The constraints of the output voltages of the DER systems are the same as the constraints in Table I, whereas the lower and upper bounds of the output power and source currents of the DER systems are 0 W, 212 W, 0 A, and 10 A, respectively. The switching frequency of the grid-connected boost converters is 100 kHz. The communication delay is about 0.01 s. The line resistances, current sink, and tuning parameters of the proposed control strategy in different scenarios are provided in Table IV. The droop coefficient (i.e., $R_{{\rm d}i}$) and tuning coefficients of the controllers (i.e., $K_{{\rm P}i}$, $K_{{\rm I}i}$, $K_{{\rm P1}i}$, $K_{{\rm I1}i}$, $K_{{\rm P2}i}$, and $K_{{\rm I2}i}$) are identical for all the DER. The line resistances of the DER systems are changed by adding high-current chassis amount resistors (i.e., TGHLVR100JE, TGHLVR500JE, and TGHLV1R00JE) to validate the effectiveness of the proposed control strategy in different scenarios. The digital signal processer (DSP) Delfino TMS320F28379D from Texas Instrument is adopted as the controllers for the DER systems. The conversion loss coefficients of are determined based on the input and output voltages and currents of the DER systems. The converter loss curves of the three grid-connected boost converters are plotted in Fig. 16(b). Apparently, the converter loss are quadratic functions of the output currents of the DER systems. The conversion loss coefficients of the DER1, DER2, and DER3 are $a_1 = 1.161$, $b_1 = 0.730$, $c_1 = 1.693$, $a_2 = 0.641$, $b_2 = 0.547$, $c_2 = 5.260$, $a_3 = 1.693$, $b_3 = 5.26$, and $c_3 = 3.54$, respectively. In Scenarios 1

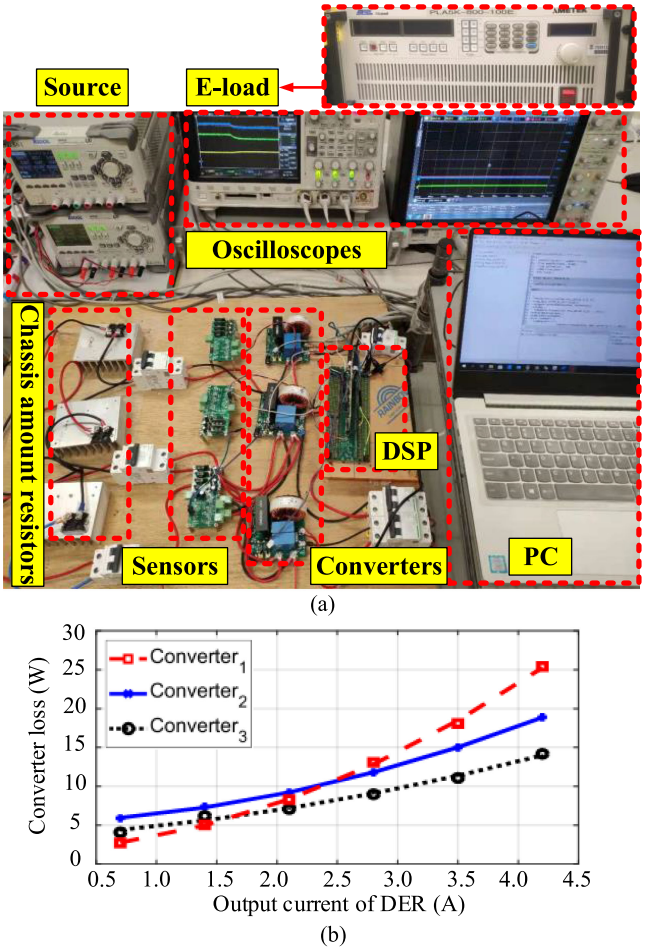

Fig. 16. (a) Test bench and (b) converter loss versus output currents of the DER systems in experiment.

TABLE IV
DETAILS OF THE THREE SCENARIOS IN EXPERIMENT

Scenario	Line resistances and current sink				Controller parameters						
	$R_1(\Omega)$	$R_2(\Omega)$	$R_3(\Omega)$	I_{tol}(A)	$R_{df}(\Omega)$	K_{Pi}	K_{Ii}	K_{P1i}	K_{I1i}	K_{P2i}	K_{I2i}
1	0.53	2.53	—	4.75	0.05	0.02	0.4	0.025	0.2	0.05	0.1
2	0.1	0.1	—	6.9	0.05	0.02	0.4	0.025	0.2	0.05	0.1
3	0.53	2.53	1.26	4.75	0.05	0.02	0.4	0.025	0.2	0.05	0.1

and 2, only DER1 and DER2 systems are adopted. In Scenario 3, all the three DER systems are penetrated.

A. Scenario I

In scenario I, the conventional control strategy and the proposed control strategy are adopted during the period from 0 to 2 s and from 2 to 5 s, respectively. The total output current is 4.75 A (i.e., $I_{\text{tol}} = 4.75$ A). Fig. 17 shows the waveforms of current allocation coefficients, Lagrange multiplier, output voltages and currents of the DER systems, output power of the first DER system, and distribution power loss of the dc microgrid. Here, the output voltages and currents are directly measured by the probes. The output power is calculated and plotted using the oscilloscope DSO-X-3034A from the Agilent Technologies. The

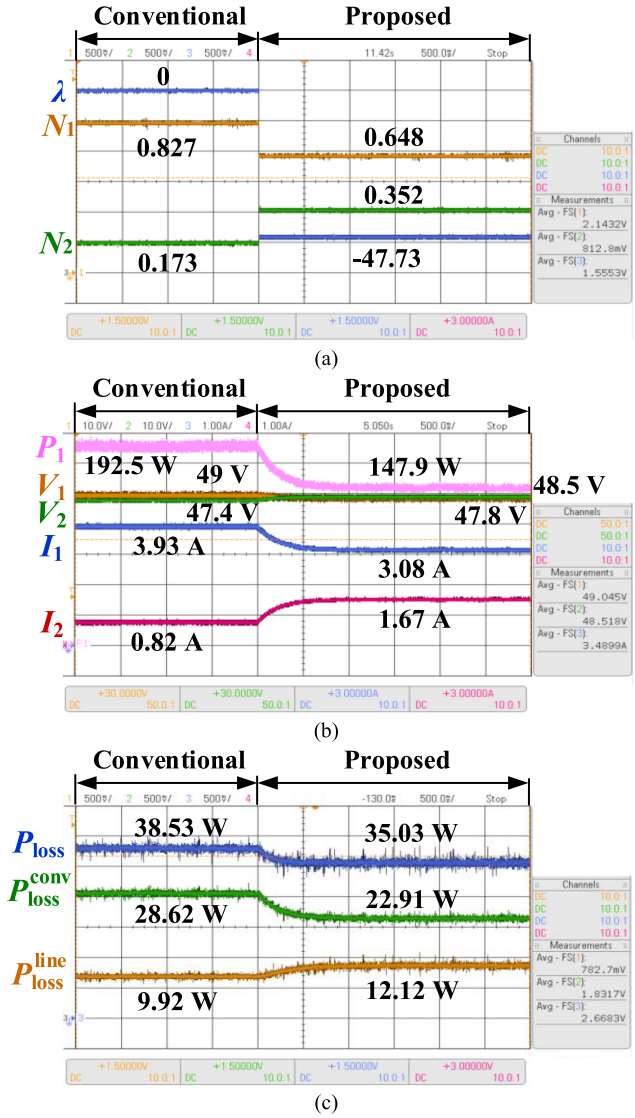

Fig. 17. Waveforms of the (a) current allocation coefficients and Lagrange multiplier, (b) output voltages, currents and power of DER systems, and (c) distribution power loss of the dc microgrid for the scenario I.

current allocation coefficients, Lagrange multiplier, distribution power loss, line loss, and converter loss are output via the digital-to-analog pins of the DSP. When the proposed control strategy is adopted at the 2 s, the Lagrange multiplier is calculated to be –47.73 and the corresponding current allocation coefficients are 0.648 and 0.352, respectively, as shown in Fig. 17(a). Based on the total output current and the current allocation coefficients, the output current references of the two DER systems can be calculated as 3.078 and 1.672 A, respectively. The measured output currents of the DER systems are 3.08 and 1.67 A, as shown in Fig. 17(b). Obviously, the output currents of the DER systems are well regulated by the adaptive droop control to track the references. The output voltages of the DER systems being controlled by the proposed control strategy are 48.5 and 47.8 V. Both the output voltages are controlled within the tolerances. The output powers of the DER systems being controlled by the proposed control strategy are 147.9 and 81 W [only the output

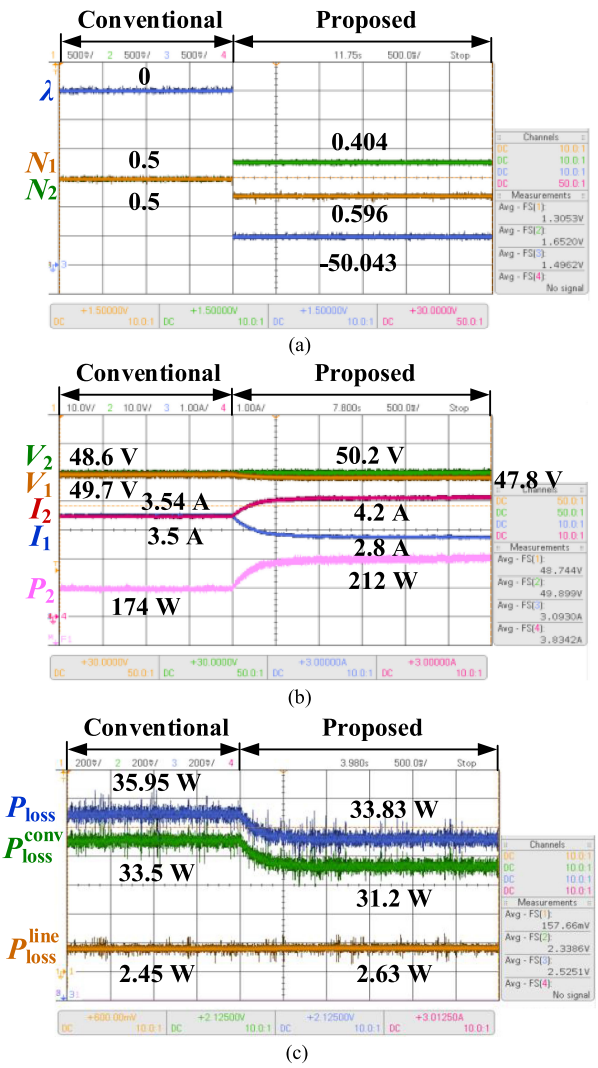

Fig. 18. Waveforms of the (a) current allocation coefficients and Lagrange multiplier, (b) output voltages, currents and power of DER systems, and (c) distribution power loss of the dc microgrid for the scenario II.

power of DER1 is shown in Fig. 17(b)]. Apparently, the output powers are also controlled within the limits. The distribution power loss for the two control strategies are 38.53 and 35.03 W, respectively.

B. Scenario II

In scenario II, the conventional control strategy and the proposed control strategy are adopted during the period from 0 to 2 s and from 2 to 5 s, respectively. The total output current is 7.0 A (i.e., $I_{\text{tol}} = 7.0$ A). The waveforms of the current allocation coefficients, Lagrange multiplier, output voltages, and currents of the DER systems, output power of the first DER system, and distribution power loss of the dc microgrid, are shown in Fig. 18. The Lagrange multiplier is –50.043 and the corresponding current allocation coefficients are 0.404 and 0.596, respectively, as shown in Fig. 18(a). Then, the output current references of the two DER systems can be calculated to be 2.788 and 4.212 A, respectively. The measured output currents of the DER systems

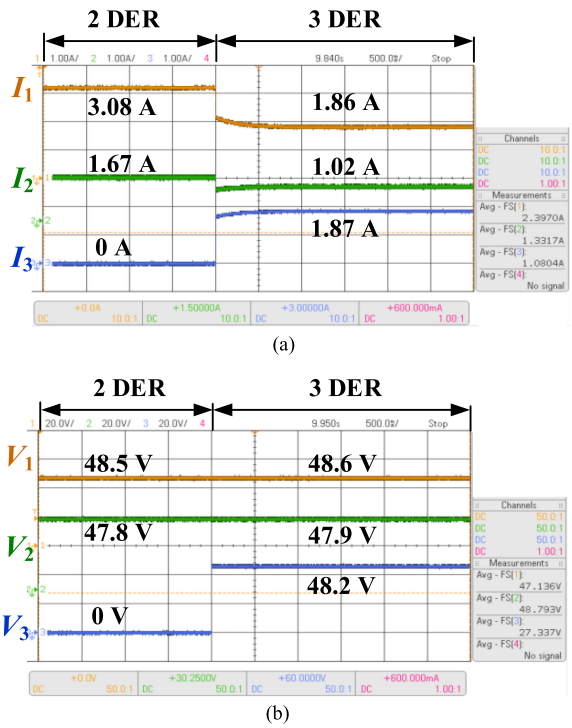

Fig. 19. Waveforms of the (a) output currents and (b) output voltages of the DER systems when the third DER is connected.

are 2.8 and 4.2 A, as shown in Fig. 19(b). Apparently, the errors between the output current references and the measured output currents are quite small. The output voltages of the DER systems controlled by the proposed control strategy, i.e., 47.8 and 50.2 V, are within the tolerances. The output power of the DER systems controlled by the proposed control strategy are 134 and 212 W [only the output power of DER2 is shown in Fig. 17(b)]. Obviously, the output power of DER2 is clamped at the boundary of 212 W. The distribution power loss of the microgrid controlled by the conventional control strategy and the proposed control strategy are 35.95 and 33.83 W, respectively.

C. Scenario III

Scenario III is set up based on scenario I by connecting the DER3 into the dc microgrid. The controller parameters of the newly connected DER system are identical to the controller parameters of the other two DER systems. Fig. 19 shows the waveforms of the output currents and voltages of the DER systems controlled by the proposed control strategy when the third DER system is connected. The output currents are reallocated to a new steady state, while the total output current remains at 4.75 A (i.e., $I_{\text{tol}} = 4.75$ A). The output voltages of the three DER are 48.6, 47.9, and 48.2 V, respectively. All the output voltages are controlled within the tolerances. Then, the conventional control strategy is adopted for the three DER systems for comparisons. Fig. 20 shows the waveforms of current allocation coefficients and distribution power loss. The current allocation coefficients of the proposed control are 0.3918, 0.2148, and 0.3934 during the period from 0 to 2 s, while the current allocation coefficients of

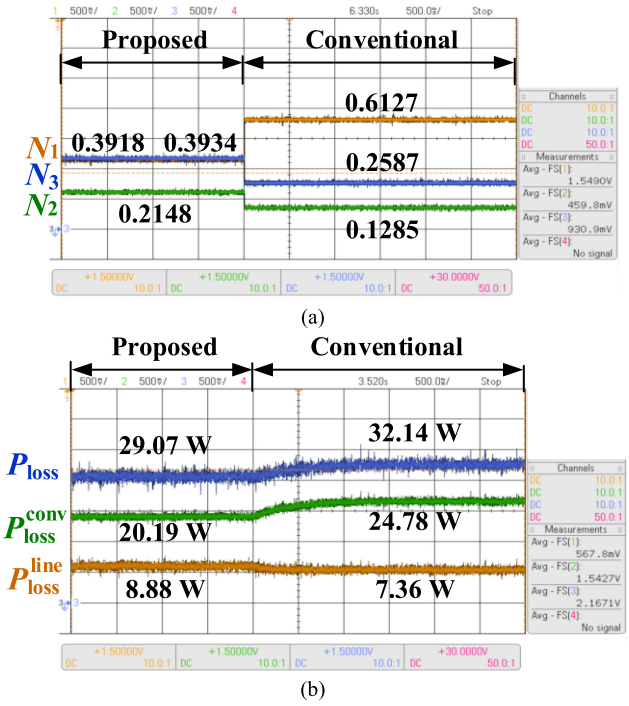

Fig. 20. Waveforms of the (a) current allocation coefficients and (b) distribution power loss of the three DER systems for the scenario III.

TABLE V
DETAILS OF THE THREE SCENARIOS IN EXPERIMENT

Scenario	Conventional P_{loss} (W)	Proposed P_{loss} (W)	Loss reduction (%)
1	38.53	35.03	9.08
2	35.95	33.83	5.9
3	32.14	29.07	9.55

the conventional control are 0.6127, 0.1285, and 0.2587 during the period from 2 to 5 s. The distribution power loss of the proposed control and the conventional control are 29.07 W and 32.14 W, respectively.

The comparisons of the distribution power loss between the proposed control strategy and the conventional control strategy in three experimental scenarios are given in Table V. The proposed control strategy can save about 9.08%, 5.9%, and 9.55% loss reduction, as compared to the conventional control strategy in scenarios I, II, and III, respectively.

VI. CONCLUSION

This article presents a Lagrange multiplier-based adaptive droop control to mitigate distribution power loss of parallel-connected DER in dc microgrids. Unlike previous studies, which consider only line loss, the proposed control strategy considers both the line loss and the converter loss. The effectiveness of the proposed three-layer hierarchical control to reduce the distribution power loss is validated by both simulation and experimental results. The three-layer control has been implemented and demonstrated successfully in hardware setups. Practical tests have confirmed that the distribution power loss of the parallel-connected DER systems in a 48 V dc microgrid can be reduced by about 9.08%, 5.9%, and 9.55%, as compared to the conventional control strategy in three scenarios.

APPENDIX

For positive real variables $x_i > 0$ ($\exists x_i \neq 0$), if they satisfy $[\sum_{i=1}^{n}(x_i - x_1)\ \sum_{i=1}^{n}(x_i - x_2)\ \cdots\ \sum_{i=1}^{n}(x_i - x_n)]^T = \mathbf{O}$, all these variables are equal as $x_1 = x_2 = \cdots = x_n$.

Proof:

By rearranging the condition in the Theorem 1

$$\begin{bmatrix} (1-n)x_1 + x_2 + \cdots + x_n \\ x_1 + (1-n)x_2 + \cdots + x_n \\ \vdots \\ x_1 + x_2 + \cdots + (1-n)x_n \end{bmatrix} = \begin{bmatrix} 0 \\ 0 \\ \vdots \\ 0 \end{bmatrix} \tag{A1}$$

which can be further simplified as

$$\begin{bmatrix} \sum_{i=1}^{n} x_i \\ \sum_{i=1}^{n} x_i \\ \vdots \\ \sum_{i=1}^{n} x_i \end{bmatrix} = \begin{bmatrix} nx_1 \\ nx_2 \\ \vdots \\ nx_n \end{bmatrix}. \tag{A2}$$

By solving (A2), all the variables are equal to each other.

REFERENCES

[1] D. J. Becker and B. J. Sonnenberg, "DC microgrids in buildings and data centers," in *Proc. IEEE 33rd Int. Telecommun. Energy Conf.*, Amsterdam, The Netherlands, Oct. 2011, pp. 1–7.

[2] L. Meng, T. Dragičević, J. C. Vasquez, and J. M. Guerrero, "Tertiary and secondary control levels for efficiency optimization and system damping in droop controlled DC–DC converters," *IEEE Trans. Smart Grid*, vol. 6, no. 6, pp. 2615–2626, Jun. 2015.

[3] M. K. Zadeh, R. Gavagsaz-Ghoachani, S. Pierfederici, B. Nahid-Mobarakeh, and M. Molinas, "Stability analysis and dynamic performance evaluation of a power electronics-based DC distribution system with active stabilizer," *IEEE J. Emerg. Sel. Topics Power Electron.*, vol. 4, no. 1, pp. 93–102, Mar. 2016.

[4] J. Ma, F. He, and Z. Zhao, "Line loss optimization based OPF strategy by hierarchical control for DC microgrid," in *Proc. IEEE Energy Convers. Congr. Expo.*, Montreal, Canada, Sept. 2015, pp. 6212–6212.

[5] Y. Jiang, Y. Yang, S. C. Tan, and S. Y. R. Hui, "Adaptive current sharing of distributed battery systems in DC microgrids using adaptive virtual resistance-based droop control," in *Proc. IEEE Energy Convers. Congr. Expo.*, Baltimore, USA, Sep. 2019, pp. 4262–4267.

[6] K. Natori, T. Tanaka, Y. Takahashi, and Y. Sato, "A study on high-efficiency floating multi-terminal power flow controller for next generation DC power networks," in *Proc. IEEE Energy Convers. Congr. Expo.*, Cincinnati, USA, Oct. 2017, pp. 2631–2637.

[7] E. Candan, P. S. Shenoy, and R. C. Pilawa-Podgurski, "A series-stacked power delivery architecture with isolated differential power conversion for data centers," *IEEE Trans. Power Electron.*, vol. 31, no. 5, pp. 3690–3703, May 2016.

[8] M. Farasat and A. Arabali, "Voltage and power control for minimising converter and distribution losses in autonomous microgrids," *IET Gener., Transm. Distrib.*, vol. 9, no. 13, pp. 1614–1620. Oct. 2015.

[9] M. Hussain, "Optimal placement of distributed energy resources in a DC microgrid with constant power loads to minimize bus voltage deviations and line losses," in *Proc. Glob. Power, Energy Commun. Conf.*, Cappadocia, Turkey, Jun. 2019, pp. 424–429.

[10] A. Garcés, "On the convergence of newton's method in power flow studies for DC microgrids," *IEEE Trans. Power Syst.*, vol. 33, no. 5, pp. 5770–5777, Sep. 2018.

[11] D. Zhang, L. Wang, J. Jiang, and W. Zhang, "Optimal power management in DC microgrids with applications to dual-source trolleybus systems," *IEEE Trans. Intell. Transp. Syst.*, vol. 19, no. 4, pp. 1188–1197, Apr. 2018.

[12] K. Rouzbehi, J. I. Candela, A. Luna, G. B. Gharehpetian, and P. Rodriguez, "Flexible control of power flow in multiterminal dc grids using dc–dc converter," *IEEE J. Emerg. Sel. Topics Power Electron.*, vol. 4, no. 3, pp. 1135–1144, Sep. 2016.
[13] T. Hong and F. de Leon, "Centralized unbalanced dispatch of smart distribution dc microgrid," *IEEE Trans. Smart Grid*, vol. 9, no. 4, pp. 2852–2861, Jul. 2018.
[14] Y. Yang, S. C. Tan, and S. Y. R. Hui, "Mitigating distribution power loss of DC microgrids with DC electric springs," *IEEE Trans. Smart Grid*, vol. 9, no. 6, pp. 5897−5906, Nov. 2018.
[15] J. Deng, Y. Mao, and Y. Yang, "Distribution power loss reduction of standalone DC microgrids using adaptive differential evolution-based control for distributed battery systems," *Energies*, vol. 13, no. 9, pp. 1–15, Jan. 2020.
[16] W. Su, S. Yun, H. Li, H. Iu, and T. Fernando, "An MPC-based dual-solver optimization method for DC microgrids with simultaneous consideration of operation cost and power loss," *IEEE Trans. Power Syst.*, to be published, doi: 10.1109/TPWRS.2020.3011038.
[17] H. Su, C. Deng, F. Guo, X. Chen, and C. Qi, "Distributed load sharing and transmission power loss optimisation for DC microgrids," *IET Control Theory*, vol. 13, no. 17, pp. 2930–2939. Apr. 2019.
[18] J. Beerten, S. Cole, and R. Belmans, "Generalized steady-state VSC MTDC model for sequential AC/DC power flow algorithms," *IEEE Trans. Power Syst.*, vol. 27, no. 2, pp. 821–829, May 2012.
[19] J. Cao, W. Du, H. F. Wang, and S. Q. Bu, "Minimization of transmission loss in meshed AC/DC grids with VSC-MTDC networks," *IEEE Trans. Power Syst.*, vol. 28, no. 3, pp. 3047–3055, Aug. 2013.
[20] J. H. Teng, S.-H. Liao, W.-H. Huang, and C. C. Chiang, "Smart control strategy for conversion efficiency enhancement of parallel inverters at light loads," *IEEE Trans. Ind. Electron.*, vol. 63, no. 12, pp. 7586–7596, Dec. 2016.
[21] W. Yuan, Y. Wang, D. Liu, F. Deng, and Z. Chen, "Efficiency-Prioritized droop control strategy of AC microgrid," *IEEE J. Emerg. Sel. Topics Power Electron.*, to be published, doi: 10.1109/JESTPE.2020.2967756.
[22] J. Ma, L. Yuan, Z. Zhao, and F. He, "Transmission loss optimization-based optimal power flow strategy by hierarchical control for DC microgrids," *IEEE Trans. Power Electron.*, vol. 32, no. 3, pp. 1952–1963, Mar. 2017.
[23] J. Ma, Y. Li, M. Zhu, and X. Cai, "Parallel operation of distributed voltage balancers for bipolar DC system with improved reliability and efficiency," in *Proc. 43rd Annu. Conf. IEEE Ind. Electron. Soc.*, Beijing, China, Oct. 2017, pp. 1387–1392.
[24] S. Boyd and L. Vandenberghe, *Convex Optimization*. Cambridge, U.K.: Cambridge Univ. Press, 2004.
[25] S. Mudaliyar and S. Mishra, "Coordinated voltage control of a grid connected ring DC microgrid with energy hub," *IEEE Trans. Smart Grid*, vol. 10, no. 2, pp. 1939–1948, Mar. 2019.
[26] H. Wang, A. M. Khambadkone, and X. Yu, "Control of parallel connected power converters for low voltage microgrid-Part II: Dynamic electrothermal modeling," *IEEE Trans. Power Electron.*, vol. 25, no. 12, pp. 2971–2980, Dec. 2010.
[27] TDHBG2500P100: 2.5kW Half-bridge Evaluation Board User Guide, Transphorm, Dec. 2017. [Online]. Available: https://www.transphormusa.com/en/document/tdhbg2500p100-user-guide/
[28] J. Zhou, M. Shi, Y. Chen, X. ChenJ. Wen, and H. He, "A novel secondary optimal control for multiple battery energy storages in a dc microgrid," *IEEE Tran. Smart Grid*, vol. 11, no. 5, pp. 3716–3725, Sep. 2020.
[29] M. Shi, X. Chen, J. Zhou, Y. Chen, J. Wen, and H. He, "Distributed optimal control of energy storages in a DC microgrid with communication delay," *IEEE Trans. Smart Grid*, vol. 11, no. 3, pp. 2033–2042, May 2020.
[30] S. Sahoo and S. Mishra, "A distributed finite-time secondary average voltage regulation and current sharing controller for DC microgrids," *IEEE Trans. Smart Grid*, vol. 10, no. 1, pp. 282–292, Jan. 2019.
[31] M. Shi, X. Chen, J. Zhou, Y. Chen, J. Wen, and H. He, "Advanced secondary voltage recovery control for multiple HESSs in a droop-controlled DC microgrid," *IEEE Trans. Smart Grid*, vol. 10, no. 4, pp. 3828–3839, Jul. 2019.
[32] Q. Xu, J. Xiao, X. Hu, P. Wang, and M. Y. Lee, "A decentralized power management strategy for hybrid energy storage system with autonomous bus voltage restoration and state-of-charge recovery," *IEEE Trans. Ind. Electron.*, vol. 64, no. 9, pp. 7098–7108, Sep, 2017.
[33] Y. Yang, Y. Qin, S. C. Tan, and S. Y. R. Hui, "Efficient improvement of photovoltaic-battery systems in standalone DC microgrids using a local hierarchical control for the battery system," *IEEE Trans. Power Electron.*, vol. 34, no. 11, pp. 10796–10807, Nov. 2019.
[34] RTE France, "Daily load curves," Jul. 2020. [Online]. Available: https://www.services-rte.com/en/view-data-published-by-rte/daily-load-curves.html

Yajie Jiang received the B.Eng. degree from the School of Electrical Engineering, Zhengzhou University, Zhengzhou, China, in 2015, and the M.Eng. degree from the School of Electrical and Electronic Engineering, Huazhong University of Science and Technology, Wuhan, China, in 2018. He is currently working toward the Ph.D. degree with the Department of Electrical and Electronic Engineering, The University of Hong Kong, Hong Kong.

His research interests include smart grid and machine drive.

Yun Yang (Member, IEEE) received the B.Sc. degree from Wuhan University, Wuhan, China, in 2012, and the Ph.D. degree from The University of Hong Kong, Hong Kong, in 2017, both in electrical engineering.

He then became a Postdoctoral Fellow with The University of Hong Kong. He is currently a Research Assistant Professor with the Department of Electrical Engineering, The Hong Kong Polytechnic University, Hong Kong, and an Honorary Research Assistant Professor with the Department of Electrical and Electronic Engineering, The University of Hong Kong, Hong Kong. He has authored or coauthored more than 40 technical papers, including 20 referred journal publications. He also has two book chapters and two U.S. patent applications. His research interests include wireless power transfer, microgrid, power electronics, and control.

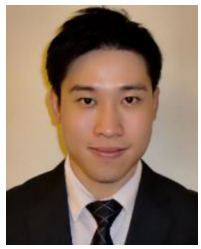

Siew-Chong Tan (Senior Member, IEEE) received the B.Eng. (hons.) and M.Eng. degrees in electrical and computer engineering from the National University of Singapore, Singapore, in 2000 and 2002, respectively, and the Ph.D. degree in electronic and information engineering from the Hong Kong Polytechnic University, Hong Kong, in 2005.

He is currently a Professor with the Department of Electrical and Electronic Engineering, The University of Hong Kong, Hong Kong. He was a Visiting Scholar with Grainger Center for Electric Machinery and Electromechanics, University of Illinois at Urbana-Champaign, Champaign, from September to October 2009, and an Invited Academic Visitor of Huazhong University of Science and Technology, Wuhan, China, in December 2011. His research interests include the areas of power electronics and control, LED lightings, smart grids, and clean energy technologies.

Shu-Yuen Ron Hui (Fellow, IEEE) received the B.Sc. (hons.) degree in electrical and electronic engineering from the University of Birmingham, London, U.K., in 1984, and the D.I.C. and Ph.D. degrees in electrical engineering from Imperial College London, London, U.K., in 1987.

Previously, he held academic positions at the University of Nottingham and University of Sydney. From 2011 to 2021, he was the Philip Wong Wilson Wong Chair Professor at the University of Hong Kong. Presently, he holds the MediaTek Professorship at Nanyang Technological University and a Chair Professorship at Imperial College London. He has published over 450 research papers including 300 refereed journal publications. Over 60 of his patents have been adopted by industry worldwide. His research interests include power electronics, wireless power, sustainable lighting and smart grid. His inventions on wireless charging platform technology underpin key dimensions of Qi, the world's first wireless power standard, with freedom of positioning and localized charging features for wireless charging of consumer electronics. He also developed the Photo-Electro-Thermal Theory for LED systems.

Dr. Hui received the IEEE Rudolf Chope R&D Award and the IET Achievement Medal (The Crompton Medal) in 2010, and the IEEE William E. Newell Power Electronics Award in 2015. He is a fellow of the Australian Academy of Technology & Engineering, US National Academy of Inventors, and Royal Academy of Engineering, U.K.